Colloidal processing and yield stress modelling towards dry pressed green bodies for transparent polycrystalline alumina.

Michael STUER[a,b] and Paul BOWEN[a,c]

a) Powder Technology Laboratory, Institute of Materials Science, EPFL, Lausanne, Switzerland
b) Alstom (Switzerland) Ltd, Brown Boveri Strasse 7, CH-5401 Baden, Switzerland
c) Corresponding author
Emails: Paul.Bowen@epfl.ch; Michael.Stuer@a3.epfl.ch

Abstract

Colloidal processing is a key aspect of modern ceramic production routes. Most formulations are found empirically and the need for a better knowledge based design of suspension formulation is of great interest for improving colloidal routes. This can be achieved by pragmatic use of interparticle potential modelling linked to rheological models for concentrated suspensions. Here we look at the details behind slurry formulation for freeze granulation of doped alumina powders for use in the production of transparent polycrystalline alumina. We take into account the variation of the attractive well depths and distance from the particle surface with thermal energy. Also the previous use of polymeric dispersants e.g. polyacrylic acid (PAA) did not show the same efficiency in the presence of dopant ions. The degree of complexation of the ions with the PAA has been investigated and shows the effect of both lowering the ionic strength and modifying the adsorption conformation. These deep insights into the subtleties of colloidal processing are discussed to provide a better basis for future formulation development.

1. Introduction

The dispersion of particles into concentrated slurries is essential in many areas of materials science and engineering and industrial processes including concretes, food technology, paints and pharmaceuticals, as well as ceramic processing. For ceramics, suspension rheology is crucial in a variety of wet processing methods (slip casting, injection moulding, screen printing, tape casting and extrusion [1]) but also indirectly for dry pressing the simplest ceramic forming method. The quality of the granules from spray drying depends on the suspension composition and rheology. To obtain high quality dense and homogeneous granules, high solid fractions and low viscosity slurries are essential. The rheological behaviour of ceramic suspensions depends on the colloidal stability, determining the degree of interaction of the particles. The colloidal stability itself depends on the interparticle forces, both the attractive forces (van der Waals) and the repulsive forces (electrostatic and steric). Most formulations for wet ceramic processing are the result of empirical approaches. Although efforts have been made to link the interparticle forces with slurry composition, it is often only treated qualitatively via zeta-potential or viscosity measurements [2] and not explicitly via interparticle interaction modelling or measurement. Although there are limitations with computing interparticle forces and potentials (i.e. particle shape), knowledge based advances in ceramic processing cannot proceed without a better understanding of the key factors determining the colloidal stability and the suspension's rheological properties. For certain forming methods such as tape casting or low pressure injection moulding [3], a certain yield stress is desired to avoid flow after passing the high shear region, so being able to predict yield stress behaviour is a real need. To move forward, a better theoretical basis on which to develop slurry formulations in a more precise manner using fundamental approaches is needed and this is illustrated in this paper in the quest to improve the processing of alumina for the production of transparent polycrystalline alumina (PCA).

The optical performance of ceramics relies on defect-free processing to allow full densification and residual porosity elimination [4-6] or at least to achieve a minimum characteristic pore size [7]. In fact, pores are highly efficient scattering centres depending on their size due to the large refractive index difference between the pore and the ceramic bulk material. For anisotropic materials such as alumina, microstructural refinement is an additional requirement to reduce inter-granular scattering due to birefringence [6]. The processing routes with best results for transparent PCA have been colloidal processing followed by natural sintering and post hot isostatic pressing (post-HIP), with real-in-line transmittances (RITs) above 60% (c.f. 86% for sapphire single crystals) [8]. More recently spark plasma sintering (SPS) has also been used to produce high RITs [9, 10]. One of the key factors for these improvements was attributed to careful colloidal processing (again an empirical approach) and the elimination of any aggregates or agglomerates.

However, one of the drawbacks for application of these transparent PCAs at an industrial level is the lack of simple processing methods such as dry pressing. In a previous study we looked at the application of freeze granulation to produce granules for dry pressing of green bodies followed by SPS sintering (more correctly referred to as pulsed electric current sintering PECS) [11]. Previous work had shown that the best RITs are achieved with doping [9, 10] and during the slurry preparation for the freeze granulation significant effects of the dopants on the slurry rheology were seen [11]. This led us to investigate on a theoretical level the interparticle forces and modelling of the yield stress [12]. Using an interparticle interaction modelling freeware (Hamaker) [13] and a yield stress model (YODEL) [14] the effect of the dopants, added as nitrates to the alumina dispersion before granulation, could be

explained and the yield stress of the alumina suspensions in the presence of Mg^{2+} and Y^{3+} ions predicted reasonably well. The results showed that it was not possible to stabilise the alumina slurries with electrostatic forces even at the relatively low ionic concentration (<0.05M) of the dopants needed for the best RITs after sintering. The strategy suggested from the theoretical work was to use a steric hindrance, a natural choice when electrostatic stabilisation does not work, which has been previously avoided to minimise possible carbon contamination during the rapid SPS sintering process which had been previously been thought to be detrimental for optical properties [15].This strategy was applied and gave reasonable reduction in yield stress (to below 5 Pa) allowing the production of granules and successful production of transparent PCA by a dry pressing processing route [11]. However the conditions used with polyacrylcic acid (PAA, 2000 and 5000 Molecular weight) only allowed solid contents of 30 vol.% which limited the quality of the granules and the resulting RITs to 53% compared to previous values of 57% when using simply freeze dried powders [9]. The reason for the inability of the PAA to sterically stabilize the suspension more adequately was attributed to possible complexation of the PAA carboxylic groups with the Mg^{2+} and Y^{3+} ions in the doped suspension formulation leading to a modification of the adsorbed conformation and a reduction in the effective adsorbed layer thickness. In the current article these interaction of PAA with the ions in solution and the consequent adsorption onto the alumina surface is looked at in more detail, to give a deeper understanding of the colloidal effects in this processing route. Also the yield stress predictions were less satisfactory at the lower ionic concentrations 0.0019M (Fig. 9 in [12]). This was attributed to effects of the position and depth of the secondary minimum from the interparticle potential used in the yield stress modelling. In the current paper we have analysed this in more detail taking into account a thermal energy contribution and the maxima and minima of the potential well, predicted from the interparticle force modelling. Also the definition of the maximum packing fraction and percolation threshold, two key parameters used in the yield stress modelling have been tested for different ionic strengths and volume fractions. This work leads once more to a better description of the suspension behaviour from a fundamental colloidal viewpoint, key for our improved understanding of colloidal processing and better designed slurry formulations.

2. Materials and methods

The powder used in this investigation was a high purity α-Al_2O_3 (Sumitomo AA04, batch YD9812, Solvadis Chemag GmbH, Germany). It has a volume median particle size D_{v50} of 440 nm (Laser diffraction, Mastersizer, Malvern, UK). The $span = (D_{v90} - D_{v10})/D_{v50}$ of the volume particle size distribution is 2.6. The total impurity concentration is less than 0.01 wt.% (≤ 5 ppm for Si, Na, Mg, Cu and Fe) and the specific surface S_{BET} = 4.2 m^2/g. The isoelectric point (IEP) of 9.86 was determined by titration with 0.5M KOH of a 2.5 wt.% powder suspension in 0.01M HNO_3 (Acousto Sizer II, Colloidal Dynamics, USA).

The different dopants have been added as nitrates, dissolved in 0.0001M HNO_3, to the suspending solution: $Mg(NO_3)_2.6H_2O$ (Aldrich), $Y(NO_3)_3.6H_2O$ (Fluka) and $La(NO_3)_3.6H_2O$ (Fluka). This allowed the precise addition of dopants using inductively-coupled plasma (ICPE-9000, Shimadzu, Switzerland) to measure the exact concentration of dopants in the solutions. Indeed, this route has been chosen because of the very fast and significant hydration of the nitrates upon contact with water vapour contained in the air, preventing a precise dopant addition using standard gravimetric methods. Adsorption of the ions onto the powder or complexation with poly-acrylic acid (PAA, M_w of 2000) was also carried out by analysing the solution composition by ICP after separation of the powder or polymer.

Rheology experiments (RheoStress RS100, Haake, Germany) were performed at different dopant cation concentrations, for varying solid load contents. Three measurement cycles were performed on each suspension with a 1 minute break between each cycle. A cycle was defined by a shear rate ramp-up curve from 0 to 200 s^{-1} in 90 seconds, a constant hold at the maximum shear rate for 60 seconds, followed by a ramp-down curve to 0 shear in 90 seconds. During the measurements, the suspensions were kept at 25°C ± 0.1°C by a thermostatic bath. A double-gap DIN 53544 and Couette-type DIN 53019 setup were used for solid loads below and above 40 vol.%, respectively. As a first approximation, the Bingham model was used to determine the yield stress by linear extrapolation to zero shear rate from the three decreasing shear rate curves.

The YODEL model [14] is used to predict the yield stress for suspensions by taking into account particle size distributions, inter-particle forces and suspension microstructure. The YODEL was developed for cements and has been successfully applied for several different systems [16-18] and is described in more detail in [14] here we give just the essential details needed for the current investigations. The YODEL predicts the yield stress using the following equation:

$$\tau = m_1 \frac{\Phi(\Phi - \Phi_0)}{\Phi_{max}(\Phi_{max} - \Phi)} \qquad \text{Eq. 1}$$

Where Φ is the solids volume fraction in the suspension, Φ_{max} is the maximum packing fraction of the dispersed powder, Φ_0 is the percolation threshold, and m_1 is a prefactor that accounts for the particle size and distribution as well as inter-particle forces:

$$m_1 = \frac{1.8}{\pi^4} G_{max} a^* u_{k,k} \left(\frac{f^*_{\sigma,\Delta}}{R^2_{v50}} \right) \qquad \text{Eq. 2}$$

with a^*, an average fixed radius of curvature for the contact points between particles; G_{max} the maximum attractive inter-particle force normalized by the radius of curvature at the contact points; R_{v50}, the median volume radius; $u_{k,k}$, a parameter taking into account the excluded volume resulting from particle agglomeration, $f^*_{\sigma,\Delta}$ is a factor taking into account the particle size distribution. For van der Waals attraction with a Hamaker constant A_0 and a minimum separation distance H, G_{max} can be then written as:

$$G_{max} \cong \frac{A_0}{12H^2} \qquad \text{Eq. 3}$$

Finally, it is important to note that a^* depends on the particle shape more than on the particle size. This takes into account that the inter-particle forces do not simply scale with the particle size, but that faceted particles may have much smaller contact curvatures than their volume equivalent spherical homologues.

3. Effect of ionic strength

3.1. Results and modelling

In the previous work [12], a good agreement between the yield stress predicted by the YODEL model and the experimental results was obtained, in particular for systems with an ionic strength of 0.0044M. However, at 0.0019 M, the model overestimates the yield stresses at the lower volume fractions, and it completely underestimates the yield stress at 50 vol.% powder for the Mg^{2+} slurries (prediction 10 Pa, measured 34 Pa). To better understand the limitations of the modelling for these conditions Mg^{2+}-doped slurries were investigated at varying ionic concentrations (Table 1) between a solid load range from 30 vol.% to 50 vol.% comparing both experimentally measured and modelled yield stresses.

Table 1: Summary of the suspension names and their ionic concentrations (and origins) for the studied Mg-doped powder suspensions.

Name	$Cation_{dopant}$ [mol/L]	$NO_3^-{}_{dopant}$ [mol/L]	$H+_{acid}$ [mol/L]	$NO_3^-{}_{acid}$ [mol/L]	$NO_3^-{}_{total}$ [mol/L]	Total ionic [mol/L]
Mg-1	0.0010	0.0020	0.0001	0.0001	0.0021	0.0031
Mg-2	0.0020	0.0039			0.0040	0.0061
Mg-3	0.0039	0.0078			0.0079	0.0119
Mg-4	0.0078	0.0157			0.0158	0.0237

In our previous study [12] the maximum packing, Φ_{max}, and the percolation threshold, Φ_0, were kept constant for specific systems, here we use them as fitting parameters for every ionic concentration, keeping constant the contact curvature of 37 nm as determined previously [12]. The minimum separation distances, *H*, were determined as previously, from the inter-particle potential calculations using Hamaker [13], whereof typical interparticle potential curves are shown in Figure 1. However, in order to also study the influence of the definition of the minimum particle separation, *H*, taken as the secondary minimum previously [12], various methods were employed (Table 2): (1) the separation at the secondary minimum (*min*), (2) the separation at the minimum energy plus thermal energy on the closer inter-particle distance side of the secondary minimum (*min*-), (3) the separation at the minimum energy plus thermal energy on the farther inter-particle distance side of the secondary minimum (*min*+) and (4) the average separation of *min*- and *min*+, which is closest to the actual average minimum separation distance under Brownian motion (*average*).

Table 2: Summary of the secondary minimum energies and the minimum separation associated with and without taking into account thermal energy of 1 *kT*.

Suspension name	Min. energy [kT]	Minimum separation [nm]			
		min	min-	min+	average
Mg-1	-1.10	56.1	44.4	200.4	122.4
Mg-2	-1.92	40.2	33.0	69.3	51.2
Mg-3	-3.42	27.3	23.4	28.1	30.8
Mg-4	-4.67	22.2	19.2	28.8	24

With these input parameters, the maximum packing and the percolation threshold have been fitted to minimize the error between the measured and the modelled yield stresses for each powder suspension using the least squares method. In each case, R^2 values above 0.999 were obtained. The results are summarized in Table 3.

Table 3: Summary of the percolation threshold (PT) and maximum packing (MP) fitting results for the different ionic concentrations of Mg^{2+} and minimum separation assumptions using the yield stresses obtained by the Bingham model.

Suspension	*min*		*min-*		*min+*		*average*	
name	**PT**	**MP**	**PT**	**MP**	**PT**	**MP**	**PT**	**MP**
Mg-1	0.31	0.50	0.34	0.50	0.08	0.50	0.14	0.50
Mg-2	0.30	0.51	0.32	0.51	0.19	0.51	0.26	0.51
Mg-3	0.16	0.54	0.19	0.55	0.06	0.54	0.12	0.54
Mg-4	0.12	0.57	0.12	0.57	0.05	0.56	0.10	0.57

It can be observed that the maximum packing is a relatively stable fitting parameter, roughly independent of the minimum separation used for the YODEL calculations. With increasing ionic concentration (from Mg-1 to Mg-4), its value increases from 0.50 to 0.57, which can be linked to the position of the secondary minimum which is reduced in return and defines the minimum particle separation (see Table 2). This tendency was verified by sedimentation experiments (Table 4). In fact the sediment densities increased from Mg-1 to Mg-3, but decreased dramatically for Mg-4. Because of the relatively high energy associated with the secondary minimum in the latter case (-4.67 *kT*), this observation is linked to kinetic effects leading to powder agglomeration and thereby increasing sedimentation volumes. This was verified by centrifugation experiments. Immediately after centrifugation, the sediment surface was rough and no difference was qualitatively observed between the sedimentation volumes. However, because the primary energy barrier for aggregation could not be overcome during centrifugation, the sedimentation volume increased over a period of one week after centrifugation, driven by osmotic pressures and double layer interactions [16, 19]. This also led to clear and smooth sediment surfaces such that the maximum sediment densities could be measured precisely at an equilibrium state. To compare the sediment densities immediately after centrifugation, filter-pressing was performed at 30 MPa. As expected, the densities by filter pressing were higher than after centrifugation.

Table 4: Relative densities in % for the sedimentation volumes for the different ionic concentrations, measurement methods and times. For filter pressing, the density was measured geometrically.

Suspension name	Sedimentation	Centrifugation	1 week after centrifugation	Filter pressing
Mg-1	48.2	~54	46.4	~56.0
Mg-2	49.2	~54	49.2	~56.0
Mg-3	50.1	~54	50.1	~55.7
Mg-4	35.8	~54	50.3	~54.0*

* sample geometry not well defined due to gelation and deformation during extraction

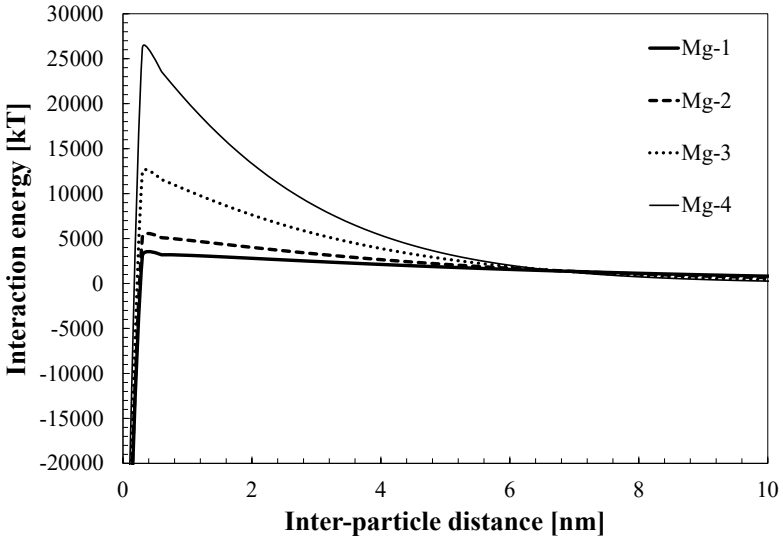

Fig. 1: Calculated inter-particle energy barriers for aggregation of alumina suspensions for various Mg^{2+} ionic concentrations. The energy barrier increases rapidly with increasing ionic strength.

The percolation thresholds in Table 3, unlike the maximum packing, are highly sensitive to the definition of the minimum separation and seem to be excessively high, especially for the Mg-1 and Mg-2 suspensions. Percolation thresholds up to 0.20 are more in keeping with previous studies [20, 21]. The percolation threshold is mostly influenced by the yield stresses obtained at lower solid loads [9]. At lower solid loads, the yield stress, and thus percolation threshold, is dominated much more by the magnitude of the absolute energy associated with the secondary minimum. Thus at low ionic concentrations, where the thermal energy is sufficient to avoid flocculation, the yield stress essentially observed at high solid loads — like for Mg-1 and Mg-2 — is due to dynamic particle collisions rather than the concept of a percolating network of flocculated particles. This could explain the excessively large percolation threshold observed for these powder suspensions. Indeed, this was verified by calculating the maximum particle packing (Φ_m) from the relative viscosity data (η_r) using the Krieger-Dougherty equation:

$$\eta_r = \left(1 - \frac{\Phi}{\Phi_m}\right)^{-n} \qquad \text{Eq. 4}$$

with Φ the particle packing of the actual powder slurry and n a fitting parameter equal to 2.5 for mono-disperse spheres.

The results of the maximum packing, calculated from the Eq. 4, are summarized in Fig 2. It can be seen that the Mg-1 and Mg-2 suspensions can be fitted with reasonable maximum packing and n values. For both, the maximum packing is estimated to be close to 0.52, which is similar to the values obtained from the fitting of the YODEL model of 0.50 and 0.51 for Mg-1 and Mg-2, respectively. For the Mg-3 and Mg-4 suspensions, the maximum packing and n values of the model curve closely fitting Mg-4 are completely unreasonable. In fact, powder aggregation — due to the secondary minimum — and the resulting exclusion volume increases the effective powder load of the slurries. This invalidates the maximum packing and n values obtained from the Krieger-Dougherty equation. This suggests that the YODEL model is better suited for aggregated powders and defines the percolation threshold for fully stabilized powder suspensions inadequately.

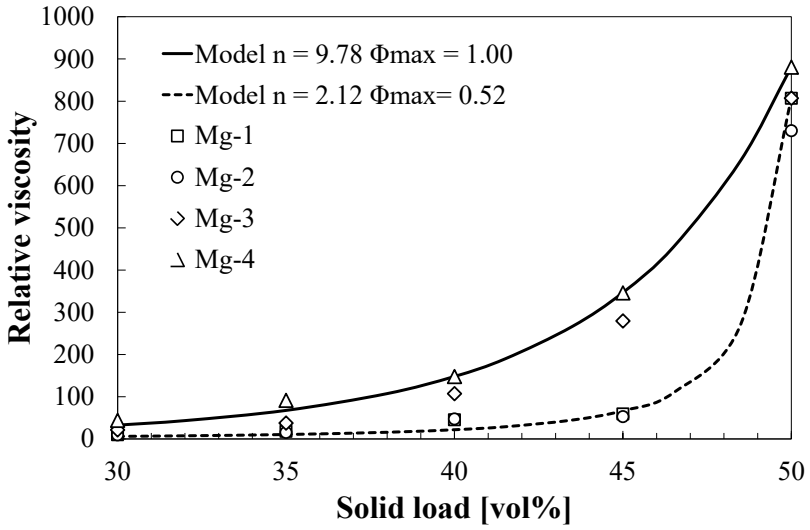

Fig. 2: Relative viscosities at shear rates of 100 s^{-1} as a function of the various solid loads for the different Mg^{2+} concentrations.

3.2. Discussion

From the results above, it can be concluded that the maximum packing is sensitive to the suspension conditions and has to be adjusted on a case-by-case basis when higher solid loading ranges (>40 vol.%) are to be included in the yield stress from the YODEL model. Determination of the maximum packing experimentally proves challenging, with filter pressing overestimating and centrifugation followed by swelling underestimating the real values. The maximum packing is, however, nearly insensitive to the minimum separation investigated over a series of conditions which took into account variations expected from thermal energy. Further investigations will be required to overcome this limitation and predict the maximum packing from interaction potential calculations. This last step will allow using YODEL as a predictive tool for the rheological properties of concentrated ceramic powder suspensions.

The percolation threshold, on the other hand, is very sensitive to both the yield stress determination method as well as the minimum separation definition. However, the percolation threshold and maximum packing are nearly identical in the absence of an attractive secondary minimum. In this case, the large variability of the percolation threshold can be explained by the dynamic nature of the measured apparent yield stress, being a dynamic inertial experimental artefact. Combining sedimentation and centrifugation tests, the percolation threshold should constantly increase from Mg-1 to Mg-4, raising a doubt about the Mg-4 values due to kinetic effects on the aggregation.

4. Interaction of dopants with PAA and effects on suspension properties

The above results (and previous results [12]) show that it is not possible to produce high volume fraction slurries with low viscosity for freeze granulation using simply electrostatic stabilization. Steric stabilization is required to improve the overall suspension stability, avoid aggregation, and thereby reduce the yield stresses. From the inter-particle energy curves, steric barriers will have to be 5-10 nm (half of the minimum separation) to eliminate the secondary minima and not increase the well depth. This would require relatively large molecular weight polymers adsorbed in a brush-like configuration (e.g. poly-acrylic acid (PAA) 10-15000 M_w). Another alternative is to increase the ionic strength and thereby allow the use of smaller adsorbed layers. However, when this was attempted [11, 12] reduced yields were achieved (<5 Pa) but only 30% volume slurries could be produced which allowed granulation but with moderate RITs after sintering by SPS [11]. Possible complexation effects with the carboxylate groups of the PAA may change the adsorbed PAA configuration, reduce the ionic concentration and modify the adsorbed layer thickness by screening ionic charges between PAA chains. The effect of dopant ions on the zeta-potential and the PAA complexation was studied to better understand the interactions and is presented in this section. In absence of organic additives, the effect of the studied dopant ions is mainly linked to their effect on the ionic strength and the resulting yield stress from the secondary minimum formation as discussed above. However, if specific adsorption occurs, they can also influence the surface charge of the particle. In the presence of PAA, the effect of dopants on the colloidal processing is more complicated. In this section, the interactions between PAA and the dopants cations as well as the powder surface will be studied in detail, PAA being an important additive for successful granulation [11].

4.1. Zeta-potential without PAA

The zeta-potential was measured as a function of the pH on the AA04 powder between pH 2 and pH 12 using HNO_3 and KOH as the titrant acid and base, respectively (Fig. 3). For the first KOH titration leg starting at pH 4, an iso-electric point (IEP) of pH 9.63 was measured with a zeta-potential around 50 mV at pH 4.

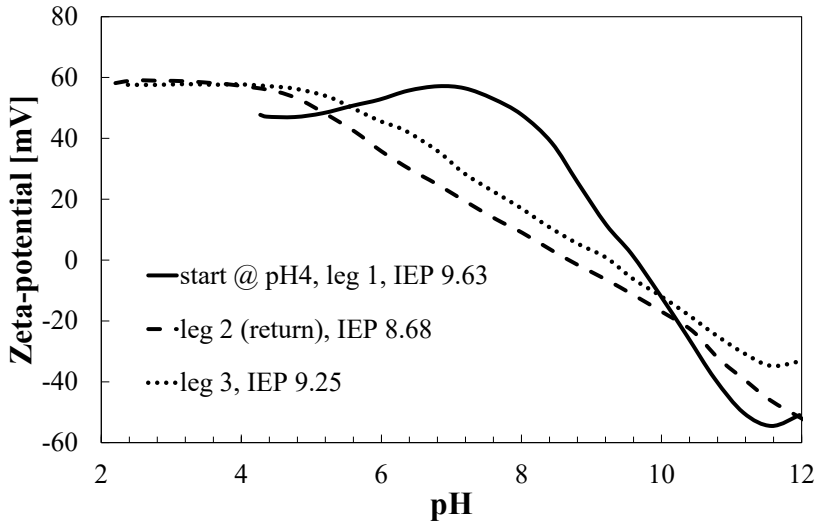

Fig. 3: Zeta-potential titration between pH 2 and pH 12 for AA04 using HNO_3 and KOH as titrating agents. No further salt was added to avoid specific adsorption changing the IEP. The start suspension was dispersed in 0.005 M HNO_3, which gave a starting pH of 4. Arriving at pH 12, a second and a third titration leg was performed using HNO_3 and KOH, respectively.

A second and a third titration leg from pH 12 to 2 and back on the same powder slurry revealed that the IEP varies during subsequent titrations between acid and basic conditions. During the reverse titration from pH 12 to pH 2, the IEP decreases from the original value of 9.63 to 8.68 before increasing again to 9.25 during the third and last titration leg from pH 2 to pH 12. The exact reasons for this have not been further investigated. However, together with the variations of the zeta-potential curves — especially between the first and the following titration legs — these results suggest that it is linked to dissolution of surface impurities (e.g. anions such as chlorine seen in TEM analysis [33]) and contaminants under basic and acid conditions. In principle, a decrease of the IEP is characterized by an anion adsorption (or cation desorption), and the reverse for the opposite case. These effects could also be linked to ions trapped in interparticle voids due to agglomeration as they pass through the IEP, the presence or late release of which could modify the observed IEP.

Titration of alumina powder slurries dispersed in 0.005 M HNO_3 at pH 4 with dopant solutions, also adjusted to pH 4, reveal a logarithmic increase of the zeta-potential with a linear increase of the suspension solution conductivity (Fig 4). Since with increasing ionic strength the zeta-potential absolute magnitude is expected to decrease, the observed increase indicates adsorption of the dopant cations. One possibility is that they replace H_3O^+, leading to higher surface charge densities and thus higher surface and zeta-potentials. This suggestion is further supported by the steeper increase observed for Y^{3+} compared to Mg^{2+} titration due to the higher cation charge. To verify this hypothesis the expected result for Mg, Y and La as a mixed solution was calculated from the single dopant zeta-titration curves, by taking 1/3 of the zeta-potential curve from Mg and 2/3 of the one from Y. A perfect fit between the measured and calculated curves was obtained (Fig. 4).

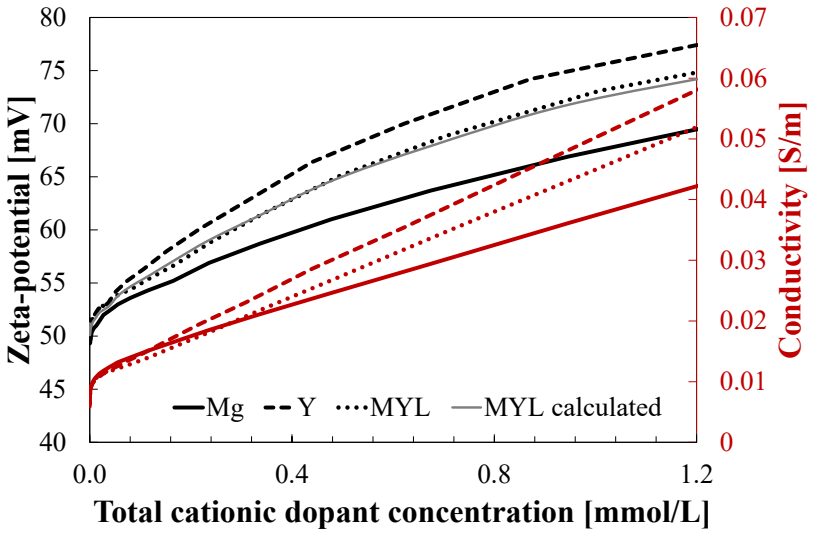

Fig. 4: Zeta-potential (black) and conductivity (red) during dopant titration in 0.005 M HNO_3 at pH 4.

Despite the observed increase in zeta-potential during dopant titration, which tends towards a maximum of 80 mV — the maximum zeta-potential measured at full protonation of the surface at pH 2 — no adsorption could be measured by ICP of the supernatant solutions. This suggests that the amount of dopants necessary to increase the zeta-potential is below the sensitivity of the ICP measurement. To estimate the amount of Mg^{2+} dopant cation adsorption required for the observed zeta-potential increase, the Grahame equation was used to calculate the surface charge density σ change [20, 21]:

$$\sigma = \sqrt{8c_0\varepsilon\varepsilon_0 RT}\,\sinh\left(\frac{zF\Phi_0}{2RT}\right) \qquad \text{Eq. 5}$$

with c_0, the bulk ionic concentration of charge z; ε, the relative dielectric constant of the medium, ε_0, the permittivity of vacuum; R, the perfect gas constant; T, the absolute temperature; F, the Faraday constant, and Φ_0, the surface potential. For simplicity, the calculation was performed using H^+ at pH 4 (0.0001 M) and dividing the required surface adsorption by a factor of two to take into account the ionic charge difference between H^+ and Mg^{2+}. For a zeta-potential increase from 50 to 70 mV, a total Mg^{2+} adsorption of $1.35 \cdot 10^{-10}$ mol/m^2 is required. For 10 g of AA04 powder in a 15 vol.% suspension this corresponds to an Mg^{2+} concentration change of 10 µg/L, which was below the practical quantification limit for these experiments.

4.2. Dopant adsorption and pH change with PAA

Complexation reactions between PAA and metal cations alter the adsorption behaviour [22-27]. The adsorption behaviour of Mg^{2+} and Y^{3+} individually in the presence of 1 wt.% PAA2000 with respect to the powder mass was measured at varying dopant additions at pH 6 and pH 9. The dispersion solutions with PAA, dopants added and pH adjusted, were prepared separately before using the required amount to disperse 20 g of AA04 powder at a solid load of 30 vol.%. The remaining dispersant solution was taken as the reference sample for the ICP measurements (e.g. to measure the total dopant addition). The powder slurries were sonicated for 10 minutes in an ultrasonic bath before rolling for one week. Before ICP, the powder was separated from the dispersing liquid by centrifugation and filtering with a syringe through a 0.02 µm syringe-filter to avoid any residual powder content. From [24] 100 hours should be sufficient for the PAA-metal ion-oxide complexes to reach a stable speciation by subsequent rearrangement reactions. The ICP revealed a net absorption of the dopants on the alumina surface in presence of PAA (Fig. 5).

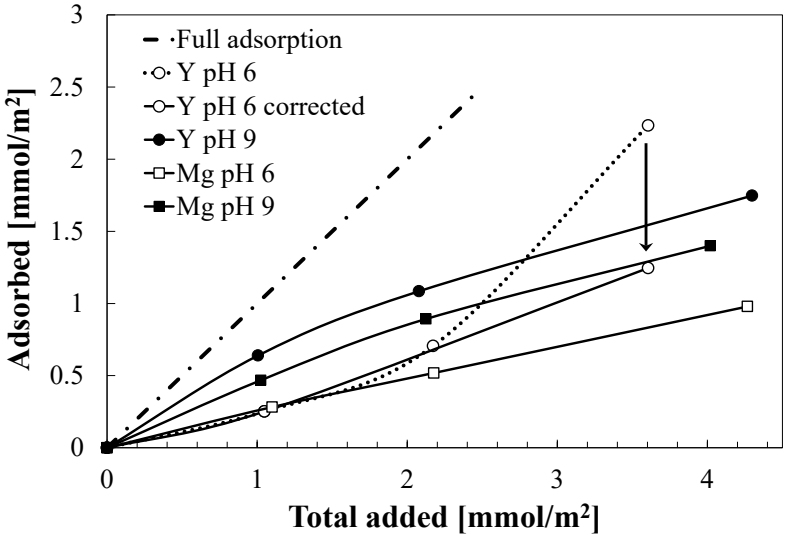

Fig. 5: Adsorption isotherms of Mg^{2+} and Y^{3+} on AA04 at pH 4 and pH 9 with 1 wt.% PAA2000 added. Precipitation of PAA/Y^{3+} complexes higher Y^{3+} concentrations at pH 6 artificially increased the adsorption isotherm and also had to be corrected by filtering the standard solution before ICP measurement.

The adsorption follows a Langmuir type adsorption isotherm. Because of the higher dissociation of carboxylate groups at pH 9 increasing the PAA electronegativity [28], the amount adsorbed is greater at pH 9 than at pH 6. Furthermore, adsorption of Y^{3+} has a higher plateau value than Mg^{2+} under similar conditions[1].

[1] The last point of the Y^{3+}-curve at pH 6 was corrected because of PAA-Y^{3+} complex precipitation. The remaining precipitates artificially increased the isotherm during filtration of the supernatant. To address the problem, the precipitates were also filtered from the reference solution. Nevertheless, the total added amount was kept constant for the recalculated isotherm because partial dissolution of the precipitates occurs upon powder

Although the order of PAA and dopant addition is expected to play a role if suspensions are prepared for immediate use, dopant-PAA complex formation prior to powder addition is not expected to modify PAA adsorption on the powder surface noticeably after aging. This was verified by preparing another series of samples as described above but this time with both Mg^{2+} and Y^{3+} added together at equal amounts (0.015 M) with varying PAA wt.% concentrations with respect to the powder mass (Fig 6). Indeed, a maximum of the dopant cations are adsorbed at 0.5 wt.% PAA addition, the required PAA amount for full AA04 surface coverage at pH 9 [29]. From the individual adsorption values, a preferential adsorption of Y^{3+} compared to Mg^{2+} in the presence of both was observed, as might have been expected from the isotherms of Fig. 5. With further PAA addition beyond the amount required for total surface coverage, the dopant adsorption decreases since a portion of them form complexes with non-adsorbed polymer.

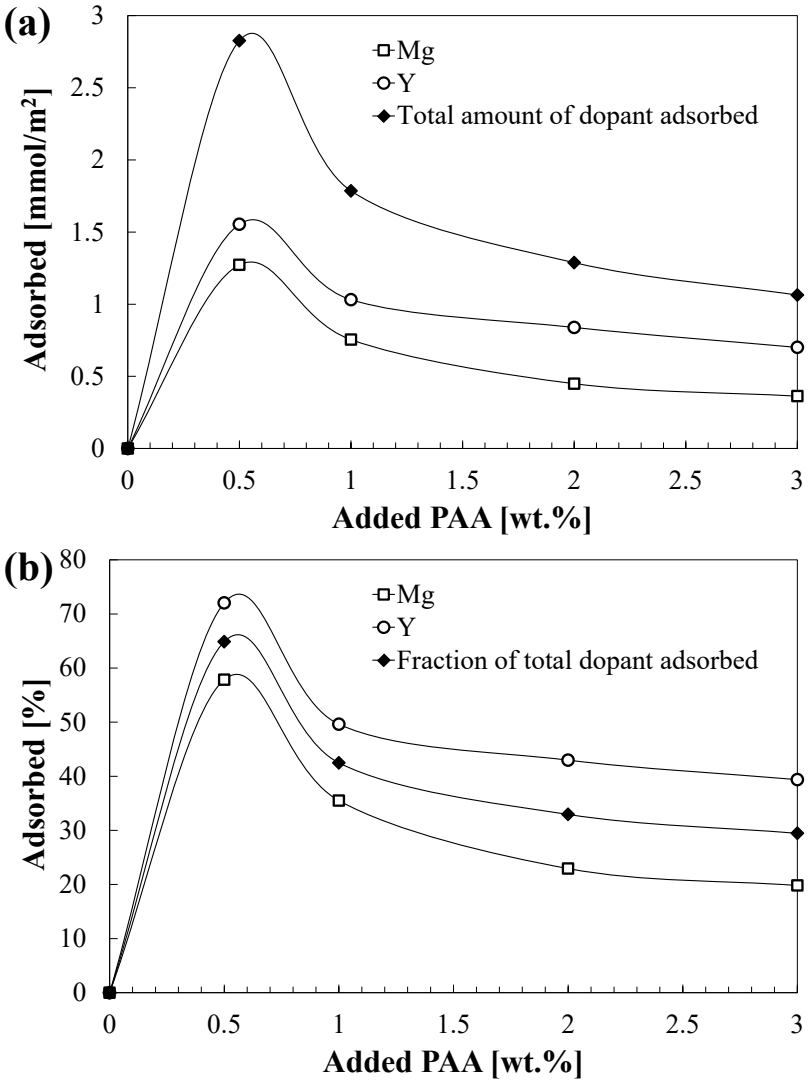

Fig. 6: Dopant adsorption as a function of the PAA wt.% with respect to the powder mass added to the powder slurries. The adsorption values are given (a) in mmol per m^2 of powder surface, (b) as a percentage of the total added amount. The total values — Mg^{2+} and Y^{3+} together — are given in addition to their individual numbers.

---

addition. Note that a small amount of precipitate formation was observed at lower Y^{3+} concentrations, which dissolved during a 15-minute ultrasonic bath treatment. For Mg^{2+}, no turbidity was observed at any concentration.

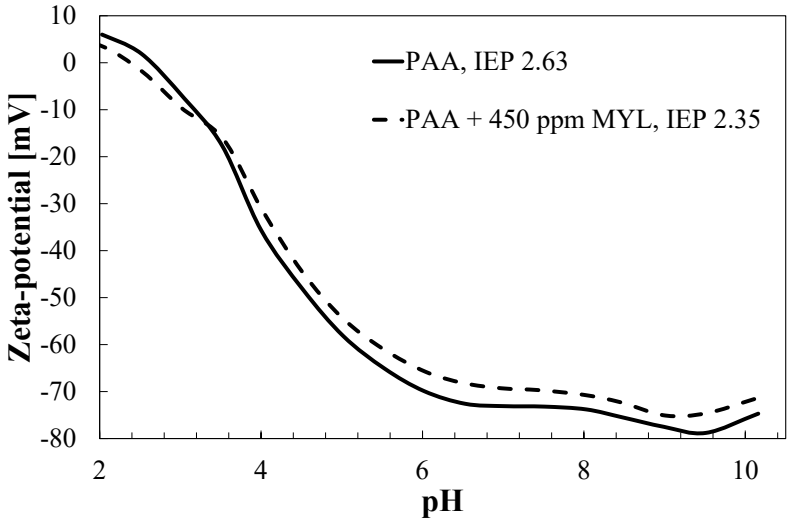

Fig. 7: pH titration curve of a 2.5 wt.% undoped and 450 ppm MYL doped AA04 slurry with 1 wt.% PAA2000 added (compared to the powder mass).

In Fig. we show how there is a strong reduction of the zeta-potential from 80 mV (in the absence of PAA) to 5 mV at pH 2 indicating that PAA dissociates and adsorbs on the powder far below its pKa value of 4.6 [28]. For the following, it shall be noted that the following observations should be dominated by interaction between PAA and the dopant cations due to the extremely low concentration of dopants used for the second titration curve in Fig. 7 (i.e. 0.2 mmol/L).

A detailed inspection of Fig. 7 reveals that the IEP is reduced from 2.63 to 2.35 in presence of dopant cations, which indicates that the dopant cations change the adsorption behaviour of PAA, increasing the amount of PAA adsorbed at low pH values — anion adsorption being required to reduce the IEP. Below the crossing point of both zeta-potential curves around a pH of 3.7, the presence of the dopant cations is expected to favour dissociation of the carboxyl groups, as has been reported to be the case from potential field interactions around surface charge sites [28, 30]. As a result of the increased dissociation, more (dissociated) PAA can adsorb on the positively charged powder surface, further reducing the magnitude of the zeta-potential on the left hand side of the crossing point. As the pH is increased towards the alkaline region, more and more carboxyl groups are dissociated [28] until at the crossing point the density of dissociated carboxyl groups is sufficient to form complexes with the metal ions without being influenced (e.g. advantageously dissociated) by the resulting potential field. Passed the crossing point (right hand side), the magnitude of the negative zeta-potential is reduced due to the presence of the complexed dopant cations, known to be preferentially located at the alumina-PAA interface [24]. The zeta-potential finally reaches a plateau value above pH 7 which subsists beyond the IEP of the powder itself (i.e. $IEP_{powder\ only}$ = 9.86), illustrating the non-electrostatic contribution involved in PAA adsorption [22, 28]. Around the powder IEP however, a small peak increase of the zeta-potential can be observed. Although small in this case — since the total PAA content is at the saturation limit — this small peak was entirely reproducible for each measurement. This peak is unlikely to be due to additional PAA dissociation, which is already fully dissociated at this pH value. A similar observation was made by Dupont et al. [29], who reported an increased PAA adsorption at the IEP of alumina in the presence of Ca^{2+} atoms. However, using large excess amounts of PAA, the magnitude of the adsorption improvement was five times higher in their case. Above the IEP, the PAA adsorption is independent of the molecular weight and dominated by electrostatic components [28]. The increased PAA adsorption at the IEP in presence of metal cations is thus believed to be linked to the effective net charge reduction of the PAA. This avoids charge

accumulation and thus electrostatic repulsion within the shear plane, improving the reported specific adsorption [28] or electrostatic adsorption on the reported site heterogeneities of the powder surface [31]. Indeed, one of these proposed mechanisms (or both) is required to explain (negative) PAA adsorption on the (negative) powder surface above the IEP.

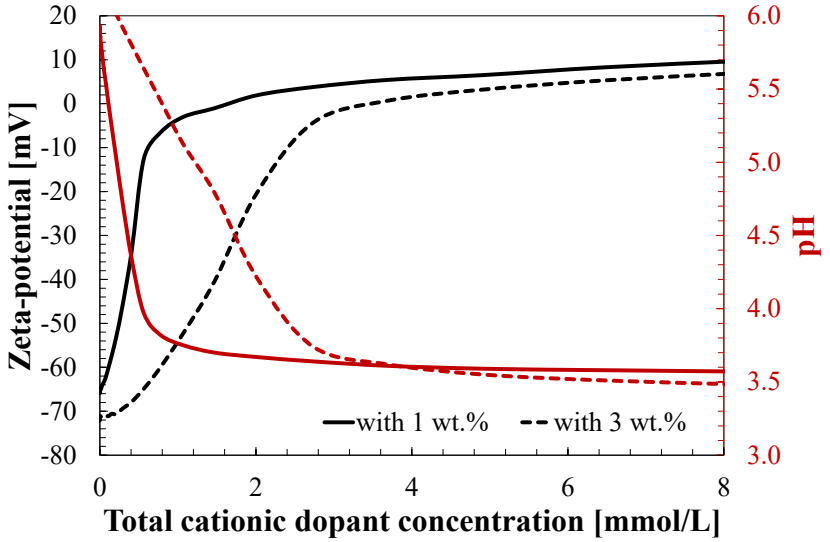

Fig. 8: Zeta-potential and pH variation of a powder slurry containing 1 wt.% and 3 wt.% PAA2000 (compared to the powder mass), respectively, during titration with a MYL-dopant solution. The pH of the 2.5 wt.% powder suspensions and of the dopant solution were adjusted to 6 before the titration experiment.

To verify the hypothesis that dopant addition — like PAA adsorption on the powder surface — can further dissociate PAA carboxyl groups (i.e. release of H^+) at a given pH to form complexes, the zeta-potential and the pH have been measured during titration with a dopant cation solution (Fig 8). The pH of both the dopant solution and the powder suspension was adjusted to a value of 6 prior to the titration experiment. Upon dopant addition, not only a zeta-potential increase but also a decrease of the pH from 6 to 3.5 can be observed, confirming H^+ release. The smaller the PAA content, the steeper the pH loss is. This illustrates that the H^+ release needs to come from carboxyl dissociation triggered by PAA-metal cation complex formation upon dopant additions. Because the pH drops from the start of the titration, the previously dissociated carboxyl groups should have fully adsorbed on the powder surface. However, since the slope of the pH drop is lower at 3 wt.% PAA, dopant addition must be accompanied by a configurational change of the PAA ad-layer. In the opposite case, a similar pH drop rate would have been expected. Thus it can be suggested that dopant addition changes the steric repulsion barrier. Furthermore, the pH drop and the maximal pH reduction depend on the metal cation charge (Fig. 9). For Mg^{2+}, the pH drop is much slower up to a maximum loss of roughly 1 unit. For Y^{3+}, however, the pH drops quickly to attain a plateau almost 3 units below the starting pH value. Therefore, trivalent metal cations do not only have a higher affinity for complexation reactions with PAA, but also a higher potential for deprotonation of the carboxyl groups. This may be due to the better charge screening capacity of Y^{3+} cations between dissociated carboxyl groups, which has been reported to increase the dissociation [22].

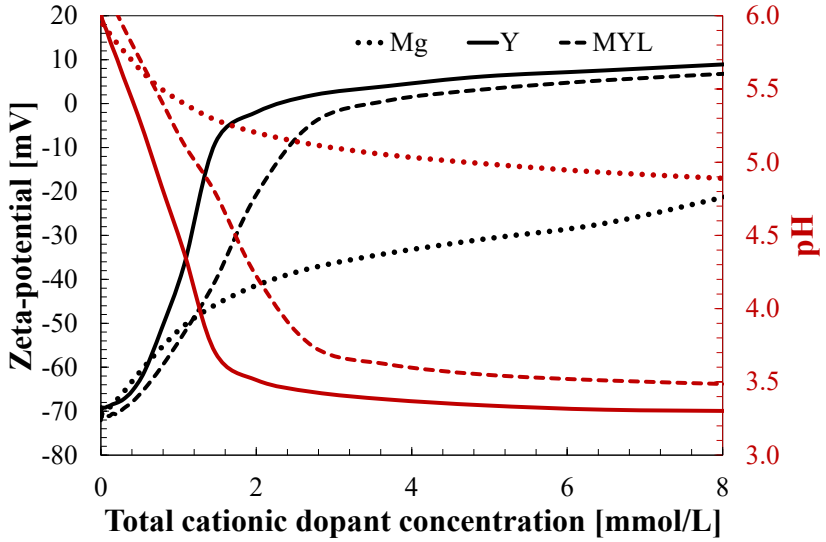

Fig. 9: Zeta-potential and pH variation during various dopant solution titrations. The pH of the 2.5 wt.% powder suspensions with 3 wt.% PAA2000 (compared to the powder mass) added and of the dopant solutions were adjusted to 6 before the titration experiment.

To determine whether a higher initial dissociation of the PAA leads to complexation plateaus without pH change before the saturation limit is reached, a similar titration was performed at pH 9 (Fig 10). However, the titrating dopant solution had to be left at pH 6.5 to avoid precipitation. Therefore a reference curve is provided by titration with the dopant solution only, without PAA addition, to be able to discuss the differences in the pH changes. As expected a plateau can be observed, which becomes wider with increasing PAA amounts. However, within the plateau a slight pH drop is observed from 9 to 8.5. The slope is less steep than without PAA and further decreases with increasing PAA content. Thus some of the H^+ present in the dopant solution must be consumed by protonation of the carboxyl groups with decreasing pH reduction. Whilst increasing the dopant concentration, once all the dissociated carboxyl groups are involved within metal complexes or surface adsorption, the pH quickly drops from pH 8.5 to approximately 7. Once more, the decreasing slope with increasing PAA content suggests involvement of an adsorption-layer conformation change.

To follow the reactivity between PAA and the dopant cations, changes of the pH can be followed upon dopant addition. The larger the final pH change, the higher the mutual affinity between the dopant cation and the PAA. To illustrate the pH change observed upon dopant cation addition, the ratio of H^+ release per dopant cation addition as a function of the pH (Fig 11) and the total dopant cation addition (Fig 12) were measured.

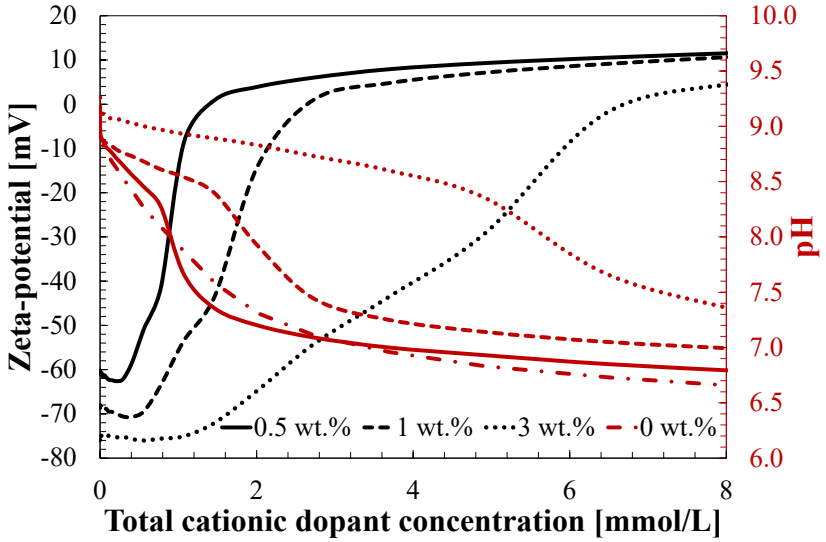

Fig. 10: Zeta-potential and pH variation of a powder slurry containing 0.5 wt.%, 1 wt.%, and 3 wt.% PAA2000 (compared to the powder mass) during titration with a MYL-dopant solution. The pH of the 2.5 wt.% powder suspensions and of the dopant solution was adjusted to 9 before the titration experiment. The pH of the dopant solution was 6.5. The pH change in the absence of PAA is provided as a reference curve.

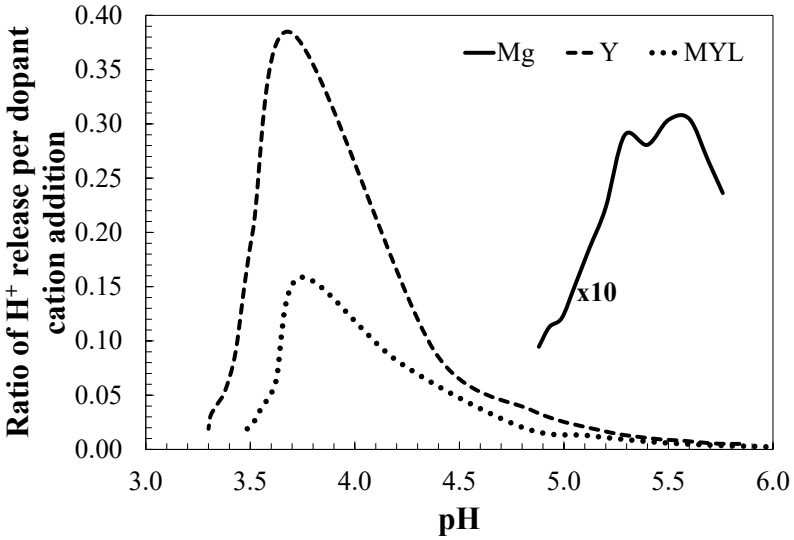

Fig. 11: Ratio of H^+ release per dopant cation addition as a function of the pH of the powder suspension. For Mg^{2+} the values have been multiplied by a factor of 10 to represent them on the same graph scale.

It can be observed that Mg^{2+} has a smaller potential to dissociate the carboxyl group because of a smaller electro-positivity than Y^{3+}. Very small amounts of carboxyl groups are deprotonated, and the pH change is small compared to Y^{3+}, for which deprotonation is important despite the trend for recombination of the carboxyl groups upon pH reduction. The fact that with Mg-Y-La addition the H^+ release peak is smaller but at a similar pH potentially indicates that the higher affinity for Y^{3+} (and probably also La^{3+}) to form complexes with PAA may lead to a cation exchange within the complexes previously formed between PAA and Mg^{2+}, and thus reduces the effective amount of H^+ released per dopant cation addition. This could also explain why the peak of the cation release is situated at higher dopant cation addition values (Fig 12), requiring an excess potential for cation exchange.

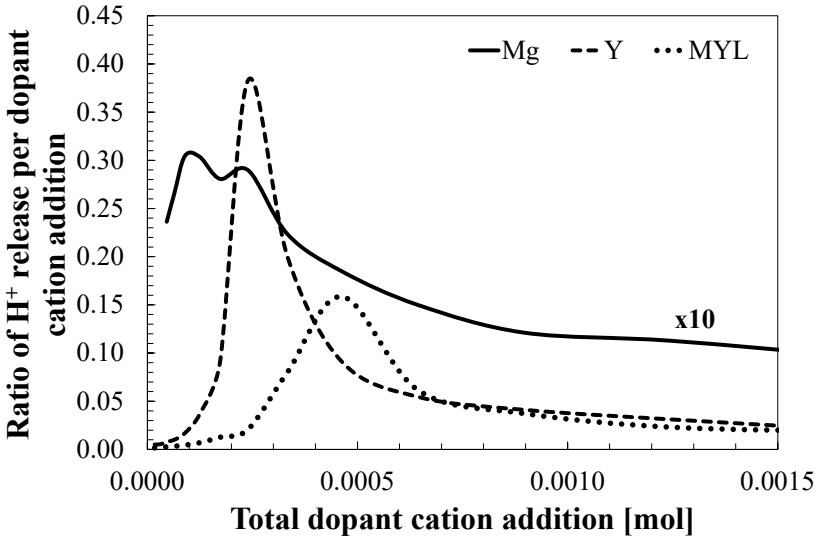

Fig. 12: Ratio of H^+ release per dopant cation addition as a function of the total dopant cation addition into the powder suspension. For Mg^{2+}, the values have been multiplied by a factor of 10 to represent them on the same graph scale.

From the ICP and zeta-potential measurements, it has been shown that there is a strong tendency for complexation between bivalent and trivalent metallic dopant cations and PAA, reducing the ionic strength of the powder slurry. Complexation increases with increasing electro-positivity of the metal cation. Because of possible complex precipitation that has been shown to be not necessarily fully reversible upon powder addition, it is beneficial to adsorb the PAA before dopant addition into the powder slurry. The complex precipitation is more pronounced at lower pH values, where the carboxyl group dissociation of PAA is lower. pH changes observed upon dopant addition showed that the metal cations can dissociate the carboxyl groups — like charged powder surfaces — beyond the normal dissociation level for a given pH. Furthermore, the presented results indicate that complexation reactions alter the adsorbed layer configuration and thickness and hence a lower steric effect than observed on alumina without the presence of the dopant ions. Consequently alternative dispersant are needed for these concentrations of dopants, such as cross-linked and comb-like copolymers (e.g. PAA–PEG [16-18, 32]) which are less sensitive to ionic strength and limit the effect of the secondary minimum.

5. Conclusions

A detailed analysis of 2 important aspects of alumina powder dispersion for the production of transparent PCA has been provided. The first was the effects of ionic concentration on the measured and predicted yield stresses. Low ionic strength and well dispersed systems could not be modelled by YODEL which requires an effective secondary minimum. For these systems the yield stresses at high solids loading (>40 vol.%) seem to be more due to dynamic interaction rather than disruption of agglomerates. A consequence of this is that for well dispersed systems the maximum packing fraction has to be evaluated case by case to be able to use the YODEL approach. This is not the case for less well dispersed systems, thus YODEL is best suited to systems presenting a strong attractive network, i.e. agglomerated systems. The effect of thermal energy (± 1kT) on the position and depth of the secondary minimum calculated using interparticle force modelling was found to have little effect on the yield stress predictions using the Yodel model, even for such low secondary minima studied in this alumina system (< 5kT).

The second aspect investigated was the complexation of PAA with the dopant ions – this was found to be significant and affected the adsorbed conformation as well as modified the ionic concentration of the suspension by complexation of the ions with PAA. This deep understanding of the colloidal processes in alumina dispersions guides us towards the use of alternative dispersants that are less sensitive to complexation when the use of dopants in the processing suspension is necessary as is the case of transparent PCA.

References

[1] F. Lange, *J.Am.Ceram.Soc.* **1989,** 72, 3; W.M. Sigmund, N.S.Bell, L. Bergström *J. Am. Ceram. Soc.* **2000,** 83, 1557.

[2] E. S. Thiele, N. J. Setter, *J.Am. Ceram. Soc.* **2000**, 83, 1407.

[3] A. Dakskobler, T. Kosmac. *J. Eur. Ceram. Soc.* **2009**, 29, 1831.

[4] R. Apetz, and M.P.B. van Bruggen. *J.Am. Ceram. Soc.* **2003**, 86, 480.

[5] A., Krell, T. Hutzler, and J. Klimke, *J. Eur. Ceram. Soc.*, **2009**, 29, 207.

[6] C. Pecharroman, et al. *Optics Express*, **2009**, 17, 6899.

[7] M. Stuer, C. Pecharroman, Z. Zhao, M. Cantoni, and P. Bowen, *Adv. Funct. Materials*. **2012,** 22, 2303.

[8] A. Krell, and J. Klimke, *J. Amer. Ceram.Soc.* **2006**, 89, 1985.

[9] M. Stuer Z. Zhao, U. Aschauer, P. Bowen, *J Eur Ceram Soc.* **2010**, 30 1335.

[10] N. Roussel, L. Lallemant, B. Durand, S. Guillemet, J. Y. C. Ching, G. Fantozzi, V. Garnier, G. Bonnefont, *J. Am. Ceram. Soc.* **2013**, 1-4.

[11] M. Stuer , Z. Zhe and P. Bowen, *J.Eur.Ceram.Soc.,* **2012**, 32, 2899.

[12] M. Stuer and P. Bowen, Adv. in Applied Ceramics **2012**, 111, 254. DOI 10.1179/1743676111Y.0000000061)

[13] U. Aschauer, O. Burgos-Montes, R. Moreno, P. Bowen, *J Dispersion Science Technology*, **2011**, 32(4), 470. *(http://hamaker.epfl.ch)*

[14] R. J. Flatt, P. Bowen, *J.Amer.Ceram.Soc.,* **2006**, 89 1244.

[15] G. Bernard-Granger, N. Benameur, C. Guizard and M. Nygren: *Scr. Mater.,* **2009**, 60, 164.

[16] Y.F. Houst, P. Bowen, F. Perche, A.Kauppi , P. Borget, L. Galmiche[i], J-F. Le Meins, F.Lafuma, R. J. Flatt, I. Schober, P. F.G. Banfill, D.S. Swift, B.O. Myrvold, B. G. Petersen, K. Reknes, *Cem. Concr. Res*. **2008**, 38 1197.

[17] A. Perrot, T. Lecompte, H. Khelifi, C. Brumaud, J. Hot, N. Roussel, *Cem. Concr. Res*. **2012**, 42, 937.

[18] M. Palacios, P. Bowen , M. Kappl, H-J. Butt, M. Stuer, C. Pecharromán, U. Aschauer, F. Puertas *Materiales de Construcción*, **2012**, 62, 489.

[19] J.A. Greathouse, S.E. Feller, and D.A. Mcquarrie, *Langmuir*, **1994**, 10, 2125.

[20] Bouvard, D. and F.F. Lange, *Acta Metallurgica et Materialia,* **1991**, 39, 3083.

[21] Velamakanni, B.V. and F.F. Lange, J. Amer. Ceram.Soc., **1991**, 74, 166.

[19] R. Buscall, et al., *Journal of Non-Newtonian Fluid Mechanics*, **1987**, 24, 183.

[21] M.N., Rahaman, *Ceramic processing and sintering,* Marcel Dekker Inc. **1995**.

[22] J. Sun, L. Bergstrom and L. Gao, *J.Am. Ceram. Soc.*, **2001**, 84, 2710.

[23] R.S. Juang and J.F. Liang,. *Journal of Membrane Science*, **1993**, 82, 163.

[24] G. Montavon et al.,. *Environmental Science & Technology*, **2004**, 38, 4312.

[25] E. Laarz et al., *J.Am. Ceram. Soc.*, **2001**, 84, 1675.

[26] O.J. Rojas et al., *J. Coll. Interf. Sci*., **1998**, 205, 77.

[27] K. Vermohlen et al. *Colloids and Surfaces a-Physicochemical and Engineering Aspects*, **2000**, 163, 45.

[28] V.A. Hackley, *J.Am. Ceram. Soc.*, **1997**, 80, 2315.

[29] L. Dupont, et al., *J. Coll. Interf. Sci*. **1993**, 161, 455.

[30] J. Blaakmeer, et al., *Macromolecules*, **1990**, 23, 2301.

[31] N.G. Hoogeveen, M.A.C. Stuart, and G.J. Fleer,. *J. Coll. Interf. Sci*., **1996**,182, 133.

[32] L. Bergstrom, A. M. Kjeldsen and R. J. Flatt:, *Cem. Concr. Res*., **2006**, 36, 1231.

[33] A. Tewari, EPFL Thesis no. 6019, **2013**.